Photochemical & Photobiological Sciences

PAPER

View Article Online
View Journal | View Issue

Cite this: *Photochem. Photobiol. Sci.*, 2015, **14**, 1346

Photoinactivation of *Candida albicans* and *Escherichia coli* using aluminium phthalocyanine on gold nanoparticles

Thandekile Mthethwa and Tebello Nyokong*

Received 18th August 2014,
Accepted 3rd June 2015

DOI: 10.1039/c4pp00315b

www.rsc.org/pps

The conjugates of aluminium phthalocyanine (complex **1**) with gold nanorods (complex **1**–AuNRs) and bipyramids (complex **1**–AuBPs) showed improved singlet oxygen quantum yields of 0.23 and 0.24, respectively, compared to that of complex **1** alone at 0.12. Complex **1** and its conjugates were used for the photoinactivation of fungi (*C. albicans*) and bacteria cells (*E. coli*). The Q band absorbances were the same for the Pc alone and when conjugated to AuNPs. The efficiency of these conjugates was evaluated by measuring the log reduction of the microorganisms (*C. albicans* and *E. coli*) after irradiation with visible light in the presence of photosensitizers. Aluminium phthalocyanine alone showed log 1.78 and log 2.51 reductions for *C. albicans* and *E. coli* respectively. However, the conjugates showed higher photosensitization with log 2.08 and log 3.34 for *C. albicans* and *E. coli*, respectively using **1**–AuBPs. For complex **1**–AuNRs log 2.53 and log 3.71 were achieved for *C. albicans* and *E. coli* respectively. The statistical analysis of the results showed that the enhanced photoinactivation observed in both microorganisms was irrespective of the shape of the nanoparticles conjugated. Photoinactivation of *C. albicans* was less than that of *E. coli* even though a higher concentration of complex **1** or its conjugates was used in *C. albicans*.

1. Introduction

Photodynamic antimicrobial chemotherapy (PACT) is an alternative method of killing microbial cells which are resistant to antibiotics.[1,2] During PACT a photosensitizer is illuminated with light of a specific wavelength resulting in the production of reactive oxygen species (ROS) which are toxic to microbial cells leading to their death. *Candida albicans* is one of the leading causes of fungal infections. It has been reported that critically ill patients suffering from HIV and pancreatitis are more inclined to fungal infections.[3]

Fungal cells are larger than those of bacteria and therefore their photoinactivation is more difficult and usually requires larger doses of light and photosensitizer to destroy them.[4] Also the cell walls of fungal cells and Gram (–) bacteria differ.[5,6] The outer membrane of Gram (–) bacteria is made up of a negatively charged lipopolysaccharide layer which becomes impermeable to neutral and negatively charged photosensitizers,[7] hence positively charged photosensitizers are more active for Gram (–) bacteria.

Phthalocyanines (Pcs) have shown great potential as photosensitizers for photodynamic inactivation of pathogens.[8–10] Phthalocyanines are good photosensitizers since they absorb visible to near infrared light, resulting in greater tissue penetration. Cationic photosensitizers have been reported to be very effective in killing both Gram (+) and Gram (–) bacteria and fungi,[11–13] hence a cationic aluminium phthalocyanine (Fig. 1A) is used in this work. The synthesis of this complex has been reported before[14] and is designated in this work as complex **1**.

We have recently reported on the improved photoinactivation activity (against *Candida albicans* and *Escherichia coli*) using a neutral platinated silicon phthalocyanine.[15] The current work reports on the potentially more effective cationic complex **1** (Fig. 1A), in combination with gold nanoparticles (AuNPs), for the photoinactivation of *Candida albicans* and *Escherichia coli*. We have also reported on the enhanced PACT activities of Pcs in the presence of spherical AuNPs against *Staphylococcus aureaus* and *Bacillus subtilis*.[16] In this work, Pcs are employed in the presence of anisotropic AuNPs (rods, AuNRs and bipyramids, AuBPs) for photoinactivation of *Candida albicans* and *Escherichia coli*.

AuNPs have been used in a variety of biological applications owing to their interesting optical and physical properties. AuNPs have been used in drug delivery,[17] biosensing,[18] imaging[19] and therapeutic applications.[20] The interesting optical properties of gold nanoparticles are brought about by their tunable surface plasmon resonance (SPR) band. AuNPs

Department of Chemistry, Rhodes University, Grahamstown 6140, South Africa. E-mail: t.nyokong@ru.ac.za; Fax: +27 46 6225109; Tel: +27 46 6038260

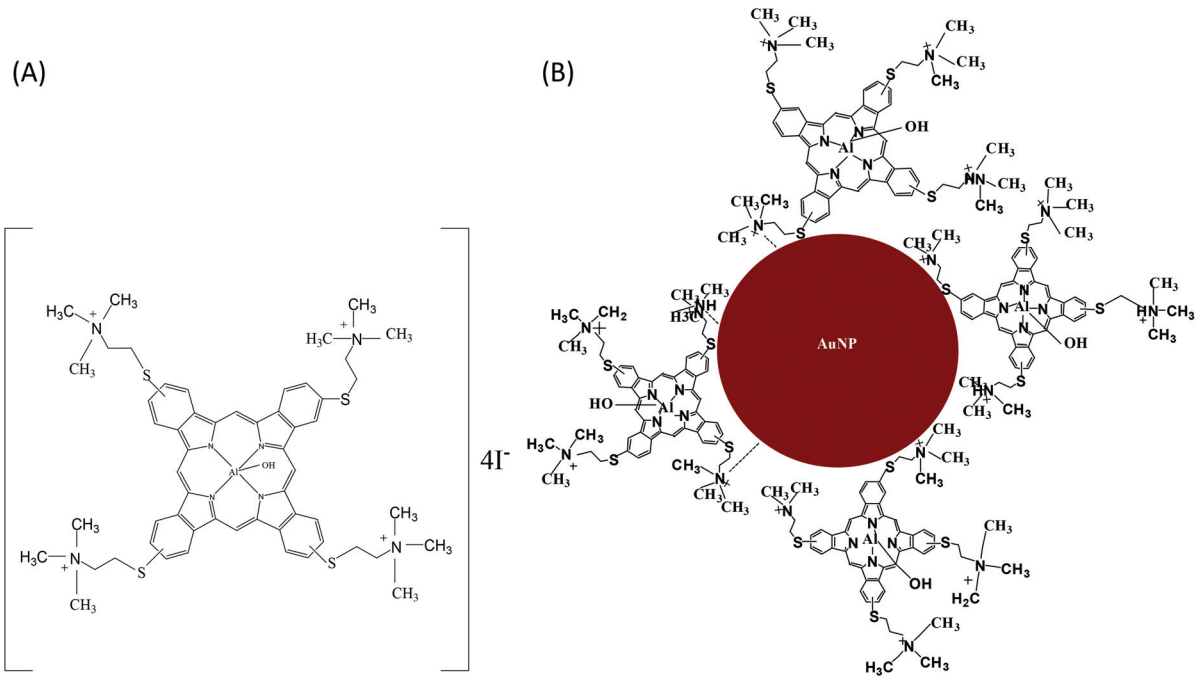

Fig. 1 (A) Molecular structure of the AlPc derivative (complex **1**). (B) Hypothetical structure based on the linking of complex **1** to AuNP.

can be prepared in different shapes and sizes and this allows the tuning of the SPR band towards near infrared which is a therapeutic window.[21,22] AuNPs improve singlet oxygen quantum yields of the photosensitizers through a heavy atom effect.[14,23,24] In addition, AuNPs on their own can act as therapeutic agents in photothermal destruction of microbial cells.[25,26] This is because when these nanoparticles are irradiated with light they can produce heat that is able to destroy the neighbouring cells. In this work aluminium phthalocyanine–gold nanoparticle conjugates are used for photoinactivation of bacteria (*E. coli*) and fungi (*C. albicans*). Gold nanorods (AuNRs) and pyramids (AuBPs) were chosen in this study because of their SPR band and high surface to volume properties which may enhance the photosensitizing behaviour of phthalocyanines. The absorption band of the AuNRs is also shifted to the red region; hence both AuNRs and complex **1** may be excited at the same wavelength. The AuBPs will not be excited at the wavelength where complex **1** is excited since the SPR band is blue shifted.

2. Materials and methods

2.1. Materials

Nutrient agar (HG 0000C1.500) and nutrient broth (HG000C24.500) were purchased from Merck. Distilled water was used for the preparation of phosphate buffer saline (PBS, pH 7.04, using NaCl, KCl, Na_2HPO_4, KH_2PO_4), agar and broth solutions. KWIK Stik *C. albicans* (ATCC 24433) and *E. coli* (ATCC 25922) crystal strains were purchased from Microbiologics. Gold(III) chloride trihydrate, sodium borohydride, trisodium citrate (99%), cetyltrimethyl-ammonium bromide (CTAB), silver nitrate, diphenylisobenzofuran (DPBF) and ascorbic acid were purchased from Sigma Aldrich. Deionized water was used for all solution preparations. The synthesis of complex **1** (Fig. 1) has recently been reported.[14]

2.2. Equipment

X-ray photoelectron spectroscopy (XPS) data were collected using a Kratos Axis Ultra DLD, using an Al (monochromatic) anode, equipped with a charge neutralizer and the operating pressure was kept below 5×10^{-9} Torr. The resolution used to acquire wide/survey scans was at 160 eV pass energy using a hybrid lens in the slot mode. The center used for the scans was at 520 eV and the width at 1205 eV, with steps at 1 eV and dwell times at 300 ms. For the high resolution scans, the resolution was changed to 10 eV pass energy in the slot mode. Transmission electron microscopy (TEM) images were obtained using a Zeiss Libra TEM 120 model operated at 90 kV accelerating voltage. TEM samples were prepared by placing a drop of the conjugate or nanoparticle solution on the sample grid and allowing it to dry before measurements. Energy dispersive X-ray spectra (EDX) were recorded on an INCA PENTA FET coupled to the VAGA TESCAM using 20 kV accelerating voltage.

The concentration of gold nanoparticles (Au^0) was determined using a ThermoElectron ICAP 6000 inductively coupled plasma (ICP) spectrometer with an optical Emission spectroscopy (OES) detector. Gold nanoparticles were digested by addition of 3 mL of aqua regia for ICP measurements. Standard calibration was achieved at concentrations ranging from

0.5 to 5 ppm. A minimum of three measurements were made for each sample of gold nanoparticles. Gold was analysed at wavelengths of 208, 242 and 267 nm.

Photo-irradiation for the antimicrobial and singlet oxygen quantum yield studies was performed using a General Electric Quartz lamp (300 W); glass (Schott) and water filters were used to filter the ultra-violet and far infrared radiations, respectively.

An interference filter (Intor, 670 nm with a band width of 40 nm) was additionally placed in the light path before the sample.

The power outputs of 25.25 mW (used for *E. coli*) or 27.75 mW (used for *C. albicans*) were measured with a Power-Max 5100 (Molelectron detector incorporated) power meter. Illumination area was 0.3 cm^2. Light intensities at 691 nm were 2.93×10^{17} and 3.22×10^{17} photons cm^{-2} s^{-1} for *E. coli* and *C. albicans* respectively for PACT studies.

X-ray powder diffraction patterns were recorded on a Bruker D8 Discover equipped with a LynxEye detector, using CuK_α radiation (λ = 1.5405 Å, nickel filter).

2.3. Synthesis of non-spherical nanoparticles

Non-spherical gold nanoparticles of various shapes were synthesized by the seed-mediated method as described by Chen *et al.*[27] The syntheses of AuNPs are described briefly below.

2.3.1. Seed solution. The AuNPs seed solution was prepared following the literature methods,[27] using CTAB instead of sodium citrate (used in ref. 27) as follows: aqueous solution of 2.5×10^{-4} M (5 mL) $HAuCl_4$ was mixed with 10 mL of a 0.1 M CTAB solution, and the mixture stirred for 2 min. Then, 0.6 mL of an ice cold aqueous solution of 0.01 M $NaBH_4$ was added, and the mixture shaken for 2 min. The solution was allowed to stand for 30 min and then used for the subsequent synthesis of differently shaped AuNPs.

2.3.2. Gold nanorods (AuNRs) and gold bipyramids (AuBPs). The growth solution was prepared according to the literature[27] by mixing 10 mL of 0.1 M CTAB, 5 mL of 2.5×10^{-4} M $HAuCl_4$ and 0.5 mL of 0.004 M $AgNO_3$ (for Au nanorods). To this solution, 0.4 mL of 0.1 M ascorbic acid was added and the reaction mixture turned colourless. Then the seed solution (12 μL) prepared above was added. The mixture was hand shaken and left undisturbed at 27 °C for 24 h. Bipyramidal gold nanoparticles were synthesized in the same way as the nanorods except that the silver concentration was increased to 0.04 M. Gold nanoparticles of a desired shape were separated from the unreacted gold and nanospheres (by-products) by centrifuging the gold solutions at 2000 rpm for 20 min. The supernatant was removed and the solid nanoparticles were dispersed in 3 mL of distilled water.

2.4. Conjugation of complex 1 to gold nanoparticles

An aqueous solution of each of the differently shaped gold nanoparticles (3 mL) was mixed with an aqueous 2 mL of complex **1** (3 mM) and stirred for 24 h at room temperature. The conjugates were purified in a size exclusion column in Bio-Beads using phosphate buffer (pH 7) as an eluent. The conjugates were then washed twice with phosphate buffer (pH 7) and centrifuged for 5 min at 2000 rpm before use for photoinactivation of microorganisms. The conjugates are represented as complex **1**–AuNRs and complex **1**–AuBPs, for conjugates of Pc with AuNRs or AuBPs, respectively.

2.5. Singlet oxygen quantum yields

Singlet oxygen quantum yields (Φ_Δ) for complex **1** and its conjugates were determined using the comparative method described before,[28] using ZnPc as a standard in DMSO, Φ_Δ = 0.67 [28] and DPBF as a singlet oxygen quencher. The absorbance of DPBF and Q band was kept at 1 and 0.5, respectively.

2.6. Biological studies

2.6.1. Preparation of microorganisms. *C. albicans* and *E. coli* cultures were grown on a nutrient agar plate prepared according to the manufacturer's specifications to obtain an individual colony. The colony was then inoculated into the nutrient broth and then placed on a rotary shaker (~200 rpm) overnight at 30 °C and 37 °C for *C. albicans* and *E. coli*, respectively. Aliquots of the culture were aseptically transferred to 4 mL of fresh broth and incubated again to the mid logarithmic phase (OD 620 nm ≈ 0.6). The bacterial cultures in the logarithmic phase of growth were harvested by the removal of the broth culture by centrifugation (3500 rpm for 5 min), washed once with PBS (10 mM) and re-suspended in 4 mL PBS. Then, the bacterial culture was diluted to 1/1000 in PBS to make a stock solution. The microorganisms in PBS were serially diluted and plated, and then the colony forming units were counted. The initial colony forming units per mL (CFU mL^{-1}) were calculated using the equation CFU mL^{-1} = number of colonies per mL plated/total dilution factor and were found to be ~10^7 and 10^8 (CFU) mL^{-1}) for *E. coli* and *C. albicans*, respectively.[29]

2.6.2. Controls. The two control experiments were performed: (1) dark controls the cells were treated with complex **1**, complex **1**–AuNPs and AuNPs without illumination. (2) Light controls had no photosensitizer but illuminated. Both controls did not show any cytotoxicity.

2.6.3. Statistical analysis. All experiments were done separately in triplicates and the results are reported as the mean values ± standard deviation of each group. Each experiment was repeated three times for each time interval. Statistical significance of more than two mean values was determined using ANOVA (analysis of variance) using error limits from at least three determinations. The difference between two means was compared using a Student's *t*-test. *P* values <0.05 were considered significant.

2.6.4. Antimicrobial studies. Preliminary experiments were performed in order to determine the appropriate light dose and photosensitizer concentration.

Photodynamic inactivation studies were conducted following the literature methods.[30,31] Briefly, *C. albicans* cells (10^8 CFU mL^{-1}) were incubated with complex **1** at a concentration of 35 μM. The mixture was incubated in an oven equipped with a shaker for 30 min in the dark at 30 °C. Then half (2 mL)

of the samples containing the Pc and cells was irradiated at the Q-band maximum of the photosensitizers in a quartz cell, using the set-up described above at different time intervals, while the other half was kept in the dark for dark toxicity studies. After irradiation, 100 μL samples were serially diluted and plated on agar plates.[31,32] A similar procedure was used for the conjugates. The concentration of complex **1** in the conjugates was adjusted by the absorbance of the Q-band. Thus the Q band absorbances were the same for the Pc alone and when conjugated to AuNPs.

Photoinactivation of *E. coli* containing an initial population of 10^7 (CFU mL^{-1}) was carried out using similar procedures but for these studies the concentration of complex **1** was reduced to 20 μM and the samples were incubated at 37 °C.

3. Results and discussion

3.1. Characterization of AuNPs and conjugates

For tetrasubstituted phthalocyanines, a mixture of four possible structural isomers was obtained. The four probable isomers can be designed by their molecular symmetry as C_{4h}, C_{2v}, C_s and D_{2h}.[33] In this study, synthesized tetra-substituted phthalocyanine compounds are obtained as isomer mixtures as expected. No attempt was made to separate them. The conjugation of the Pc to the AuNPs is not expected to be different for the isomers since they do not show any difference in their spectral behaviour.

Due to the well-known formation of Au–S bonds, complex **1** (Fig. 1) will form conjugates with AuNPs through a covalent bonding of the Pcs to the nanoparticle surface as reported before for other Pcs where the thioacetate groups were linked to AuNPs.[34] The phthalocyanine complexes are attached to the AuNPs surface by the Au–S bond due to the sulfur groups on the periphery of the phthalocyanine ring. A hypothetical representation of the conjugate (showing Au–S bonds) is shown in Fig. 1B. The number of complex **1** molecules conjugated to AuNPs will be determined below.

When the concentration of $AgNO_3$ solution was 0.004 M, AuNRs were produced. Increasing the concentration of the $AgNO_3$ solution from 0.004 M to 0.04 M favoured the formation of gold nanoparticles with a bipyramidal shape. Liu and Guyot-Sionnest[35] also observed the formation of bipyramidal gold nanostructures in the presence of silver nitrate.

Gold nanorods and gold bipyramids are both characterized by the aspect ratio (length/width) and their SPR bands can be tuned to near infra-red. Their properties depend on their longitudinal SPR bands; however AuBPs have irregular structures compared to AuNRs. The difference in these nanoparticles is due to different crystalline structures of the seeds. An irregular structure of the AuBPs may cause inhomogeneities in the field when the nanoparticles are excited and cause them to respond differently from the AuNRs. Therefore, this study compares the effect of both AuBPs and AuNRs.

3.1.1. TEM studies. The TEM image in Fig. 2A(i) shows the distribution of the as-synthesized AuNRs. The average aspect ratio (length/diameter) of the nanorods was estimated to be ~3.2, Table 1. Fig. 2A(ii) shows that upon conjugation (for **1**–AuNRs) the rods were drawn closer together showing some aggregation. The aspect ratio of the pyramidal nanoparticles was found to be 2.5, Fig. 2B(i), which increased to 2.9 upon conjugation to complex **1** (Fig. 2B(ii)).

The sizes determined from TEM were employed to determine the parameters of AuNPs such as the surface area and number of gold atoms. First, ICP OES was used to determine the total number of gold atoms per mL which was converted to moles per L using Avogadro's constant. Then the concentration of the AuNPs was employed to determine their molar extinction coefficients using Beer's law, following established methods.[36] Molar extinction coefficients were larger for AuNRs compared to those for AuBPs, Table 1.

The total number of Au atoms per AuNP (N), the surface area of AuNPs and the number of surface Au atoms (N_s) per AuNP were calculated using established methods,[37–39] assuming perfect rod-like and bipyramidal shapes. The total numbers of gold atoms, the number of surface gold atoms as well as the surface area were larger for AuBPs than those for AuNRs. The number of Pc molecules on AuNPs was also obtained using the Beer's law and the Q band absorption maximum of the phthalocyanines (assuming the extinction coefficient ($\log \varepsilon = 5.0$) does not change upon conjugation). The number of phthalocyanine molecules per nanoparticle was found to be 66 for AuNRs and 112 for AuBPs, Table 1.

3.1.2. EDS. The EDS spectrum of the gold nanoparticles in Fig. 3(A) shows the gold peaks and confirms the presence of cetyltrimethyl-ammonium bromide (CTAB) in the samples. The presence of the carbon, bromine and nitrogen peaks is due to CTAB chains that act as capping agents on the gold surfaces. The spectrum shows traces of silver in the gold nanoparticle samples which is due to silver nitrate that was used in the synthesis of the nanoparticles. The presence of the phthalocyanine in the conjugates was confirmed by the presence of the carbon, aluminium, sulphur, iodide and oxygen elements (Fig. 3(B)). A gold peak was also observed in this sample due to the gold nanoparticles. The samples contain chlorine and sodium elements due to impurities from the synthesis (PBS containing NaCl was employed in the final purification step). Silver was also detected in the conjugates.

3.1.3. XRD studies. The XRD pattern of AuNRs (as an example) is shown in Fig. 4. AuBPs gave a similar XRD pattern. The diffraction patterns were indexed to the face centred cubic crystal structure of the gold nanoparticles.

3.1.4. XPS studies. The binding of the phthalocyanine on gold nanoparticles was studied using high resolution XPS spectra. Fig. 5(A) shows the XPS spectra for S 2p analysis in which a doublet due to $2p_{3/2}$ and $2p_{1/2}$ was observed. The existence of the S 2p doublets is a result of the spin–orbit coupling.[40] The phthalocyanine alone showed two characteristic peaks at 161.0 and 162.4 eV. The $2p_{3/2}$ at 161 eV is commonly attributed to isolated sulphur or intact molecules.[41] However, for the conjugate the two main S 2p peaks shifted to higher binding energies at 162.5 and 163.7 eV, Fig. 5A(ii). The

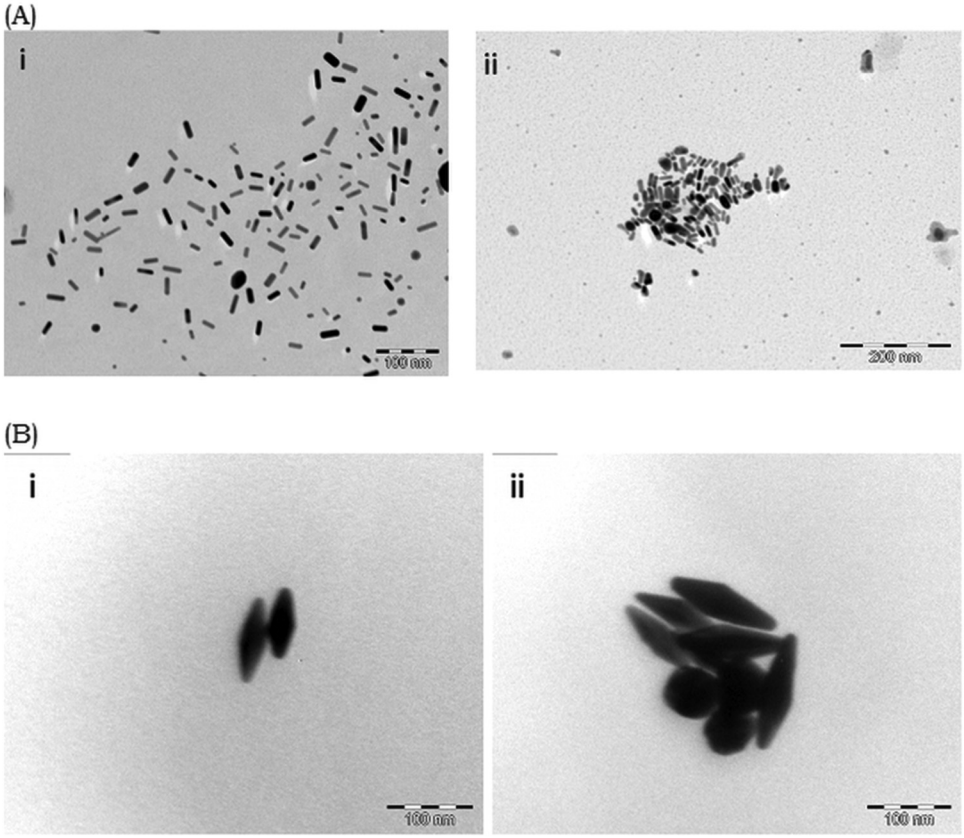

Fig. 2 TEM images of (A) AuNRs and (B) AyBPs alone (i) and conjugated to Pc (ii).

Table 1 Properties of the gold nanoparticles. Numbers in brackets represent the presence of complex **1**. N = total number of gold atoms in a nanoparticle, N_s = number of surface atoms

Sample	Surface area (nm^2)	N	N_s	Aspect ratio from TEM	ε (M^{-1} cm^{-1})	Pcs/NPs
AuNRs	552	68 397	9362	3.2 ± 0.5 (3.7)	126 808	66
AuBPs	26 231	16 430 269	444 901	2.5 ± 0.3 (2.9)	118 182	112

162.5 eV peak is due to the sulphur bonded to the gold surface while the second peak at 163.7 eV could be assigned to physisorbed molecules on the gold surface.[42–45] The shift in the binding energies is due to the loss of the electron lone pair when sulphur is adsorbed on the gold surface.

The nitrogen 1s high-resolution XPS spectrum of the phthalocyanine showed three characteristic peaks at 398.0, 400.1 and 401.7 eV, Fig. 5B(i). These peaks were attributed to C═N, pyrrolic nitrogen and the quaternary nitrogen.[45–47] Fig. 5B(ii) shows the nitrogen 1s XPS spectrum of the conjugate. There are two main characteristic peaks at 396.2 and 397.9 eV corresponding to N–Al and N–C respectively.[48] The quaternary N 1s peak disappeared upon conjugation with gold nanoparticles showing the participation of this nitrogen in the complex **1**–NR conjugates. The reaction of the quaternary nitrogen on metal nanoparticle surfaces is very common in the literature.[49–52]

The carbon 1s XPS spectra of the phthalocyanine and the phthalocyanine–gold conjugate are shown in Fig. 5C. The peaks at 282.4 and 283.7 eV were observed on the aluminium phthalocyanine for C═C and C–C and/or C–H respectively, Fig. 5C(i). The carbon 1s XPS spectrum of the phthalocyanine on gold nanoparticles showed the peaks at 283.7 and 285.0 eV which are attributed to C═C and C–C and/or C–H respectively,[53] Fig. 5C(ii). The peak shifting towards larger binding energies can be associated with loading, as suggested by Yang *et al.*[54]

3.1.5. UV-Vis absorption and fluorescence spectra. The UV-Vis spectra of gold nanoparticles are shown in Fig. 6A and B and the characteristic SPR absorption properties are reported in Table 2. The existence of multiple bands in non-spherical particles has been reported.[35] The UV-Vis spectra of complex **1**–AuNP conjugates (Fig. 6A and B) show a characteristic SPR band, which proves the presence of gold

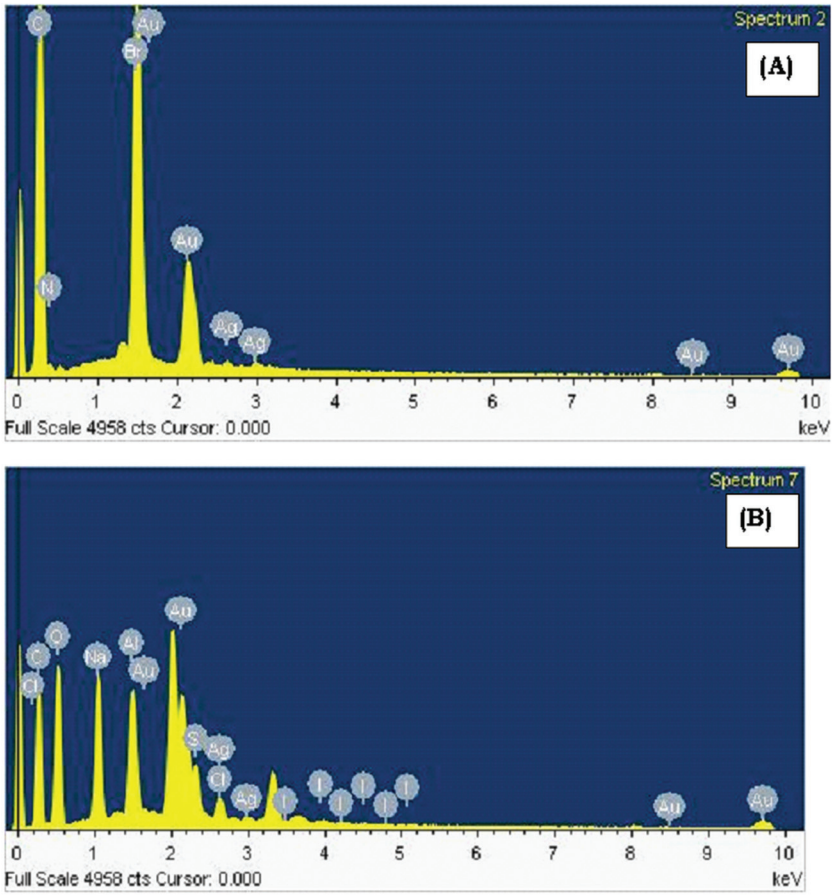

Fig. 3 EDS spectra of (A) gold nanoparticles and (B) complex **1**–gold nanoparticles.

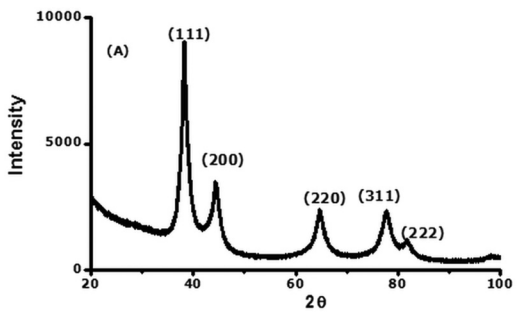

Fig. 4 XRD pattern of AuNRs.

nanoparticles in the samples. The SPR peaks in the conjugates are slightly red shifted compared to AuNPs alone, Table 2. The bathochromic shifts are due to slight aggregation of these nanoparticles in the conjugates, as reported before.[55]

The conjugation of gold nanoparticles resulted in the red shifting, Table 2, and broadening of the Q-bands of complex **1** in DMSO (Fig. 6A and B). Broadening of the phthalocyanine Q-band absorption in the presence of nanoparticles such as Au was attributed to a tight packing of the phthalocyanines on the nanoparticle.[34]

It is possible that the red shifts observed in the Q band of the Pc in the presence of the AuNP may be due to the longitudinal dipole moment arrangement of both, which is known to result in red shifts for other chromophores.[56]

Complex **1** is soluble in water, and studies conducted in water are preferable. However this complex is highly aggregated in aqueous media as reported before,[14] making it difficult to undertake the photochemical and photophysical studies, since aggregates are photoinactive. The aggregation remained in the presence of AuNPs, Fig. 7. Aggregation in Pcs is characterized by the presence of a blue shifted band near 630 nm due to the aggregate and another band at lower energies due to the monomer.[57]

3.1.6. Singlet oxygen quantum yields. Fig. 8 shows the photodegradation of the singlet oxygen quencher DPBF. An increase in singlet oxygen quantum yields in the presence of gold nanoparticles was observed which shows the influence of the heavy atom effect exerted by the gold nanoparticles (Table 2). There is not much difference between the effects of AuNRs or AuBPs on the singlet oxygen quantum yield for complex **1**. The increase in singlet oxygen quantum yields

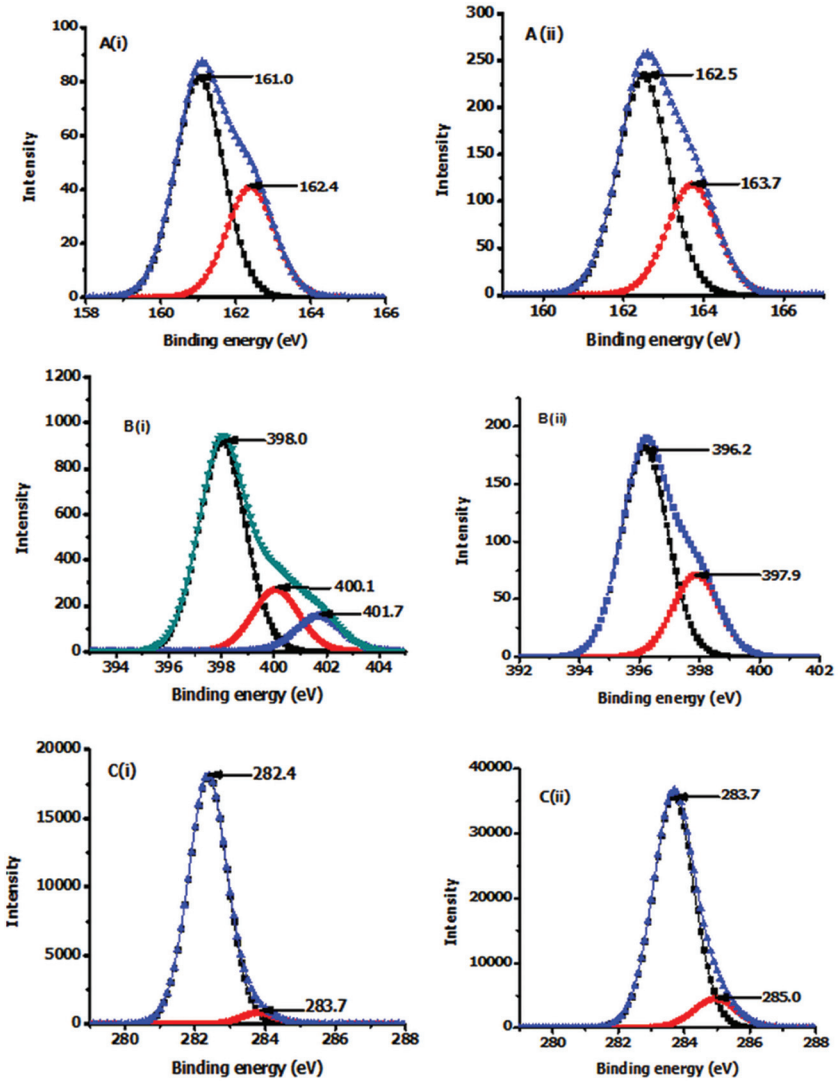

Fig. 5 High resolution XPS spectra of (A) sulphur 2p, (B) nitrogen 1s and (C) carbon 1s; (i) complex **1** and (ii) complex **1**–gold nanorod conjugates.

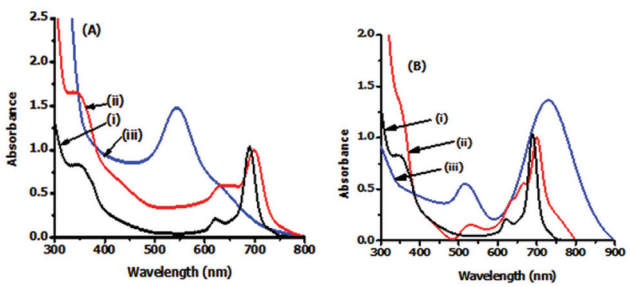

Fig. 6 UV-Vis spectra of (A) AuBPs and (B) AuNRs, and their conjugates; (i) complex **1** and (ii) complex **1**–gold nanoparticle conjugates and (iii) gold nanoparticles in DMSO.

shows that the molecule may be used for PDT applications in the presence of variously shaped AuNPs. Quantification of singlet oxygen in aqueous media was not possible due to aggregation.

3.2. Photoinactivation studies

The photosensitizer–gold nanoparticle conjugates have the ability to enhance photoinactivation of bacteria through a synergistic effect of photothermal (AuNPs) and photodynamic (Pcs) therapies. Gold nanoparticles can also enhance the photoinactivation process by increasing the generation of reactive oxygen species (ROS).[58] Tuchina *et al.* reported the enhanced photodynamic activity of the gold nanoparticles–indocyanine green dye for photoinactivation on *Staphylococcus aureus*.[59] Maliszewska *et al.* reported enhanced photoinactivation of *S. epidermidis* by methylene blue–gold nanoparticles conjugate without any significant effect from the gold nanoparticles alone (without methylene blue).[60]

The biological studies in this work were performed by irradiating the complex alone or in the presence of AuNRs at wavelengths where both absorb. AuBPs were also investigated even though their absorption peak does not match the absorption of complex **1**, Fig. 6. The contribution of AuNRs and AuBPs

Table 2 Spectral properties of complex **1** and complex **1**–AuNP conjugates in DMSO

Conjugate	λ_{Abs} [a]/nm	SPR[b]/nm	Φ_Δ
Complex **1**	691	—	0.12
Complex **1**–AuNRs	702	530 (513, 749)	0.23
Complex **1**–AuBPs	704	551 (548)	0.24

[a] λ_{Abs} = Absorption maximum. [b] Numbers in brackets refer to the SPR bands for AuNPs alone.

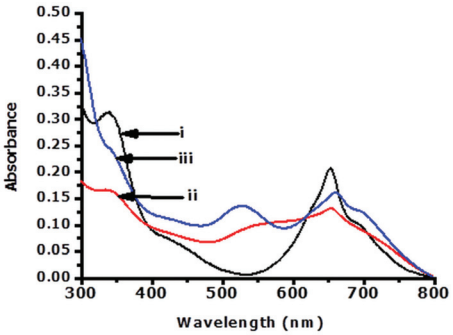

Fig. 7 UV-Vis spectra of complex **1** mixed with AuNPs in aqueous media: (i) complex **1**, (ii) complex **1**–AuNBPs, (iii) complex **1**–AuNRs.

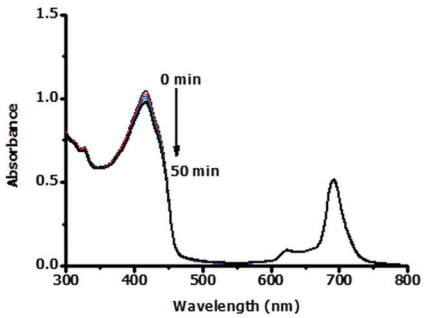

Fig. 8 Photooxidation of DPBF in the presence of complex **1** in DMSO.

towards the PDT activity of complex **1** was (in addition to the possible photothermal effect of AuNRs at the excitation wavelength) made possible by enhancing singlet oxygen through the heavy atom effect.

3.2.1. Photoinactivation of *Candida albicans*. The PACT efficiency of complex **1** and its conjugates with AuBPs and AuNRs was evaluated by applying a power density of 92 mW cm^{-2}. Fig. 9(A) shows the survival curves for *C. albicans* in which the colony forming units were measured against light fluence. The number of colony forming units (CFU) decreased with increasing light fluence. Complex **1** alone gave a 1.78 CFU log reduction (p = 0.003) (Fig. 9A and Table 3). For the conjugates, 2.08 (p = 0.002) and 2.53 log (p = 0.001) reductions were achieved for complex **1**–AuBPs and complex **1**–AuNRs, respectively under the same conditions, Table 3. Statistical analysis showed no significance difference between the two conjugates (complex **1**–AuBPs and complex **1**–AuNRs) (p = 0.33).

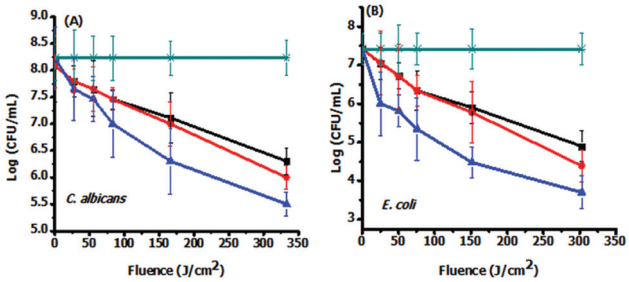

Fig. 9 Survival curves of (A) *C. albicans* (irradiance 92 mW cm^{-2}) and (B) *E. coli* (irradiance 84 mW cm^{-2}). (■) Complex **1** alone, (●) **1**–AuBPs, (▲) **1**–AuNRs and (×) light control (with light in the absence of complex **1** or its conjugates); the error bars represent standard deviation of three independent experiments.

Table 3 Summary of log CFU reduction values

Photosensitizer	*C. albicans*	*E. coli*
AuBPs	0.26 (p > 0.05)	0.68 (p > 0.05)
AuNRs	0.47(p > 0.05)	0.77 (p > 0.05)
Complex **1**	1.78 (p = 0.003)	2.51 (p = 0.03)
Complex **1**–AuBPs	2.08 (p = 0.002)	3.34 (p = 0.004)
Complex **1**–AuNRs	2.53 (p = 0.001)	3.71 (p = 0.001)

For photoinactivation with AuBPs and AuNRs alone (without complex **1**), an insignificant reduction of 0.26 and 0.47 log (p > 0.05), respectively, was achieved, Table 3 (figures not shown). Thus, the photothermal effect (for AuNPs) of the nanoparticles was negligible; however, conjugation with a phthalocyanine produced an enhanced photoinactivation which may be associated with the heavy atom effect of the gold nanoparticles or increased production of ROS catalysed by gold nanoparticles.

3.2.2. Photoinactivation of *E. coli*. Fig. 9(B) shows the survival curve of *E. coli* after photoinactivation with complex **1**. Complex **1** is a cationic molecule (Fig. 1) and is expected to bind the cell wall of the Gram negative *E coli*. A statistically significant 2.51 log reduction (p = 0.03) was obtained for complex **1** alone (Table 3). For **1**–AuBPs and **1**–AuNRs the log reduction increased to 3.34 (p = 0.004) and 3.71 (p = 0.001) respectively, Table 3 (Fig. 9(B)). The results showed a significant increase in the reduction of *E. coli* in the conjugates compared to complex **1** alone. The p value analysis showed insignificant difference between the two conjugates (complex **1**–AuBPs and complex **1**–AuNRs) (p = 0.25).

Insignificant log reductions of 0.68 and 0.77 (p > 0.05) were obtained for AuBPs and AuNRs (gold nanoparticles without complex **1**), respectively, Table 3 (figures not shown).

3.2.3. Discussion of the photoinactivation results. It can be noted that even though AuNRs absorb within the wave-

length used in this work, they did not show any significant result of photoinactivation on their own. However, upon conjugation with complex **1** there was enhanced photoinactivation of the bacteria.

The conjugates gave a significantly higher log reduction ($p < 0.05$) compared to complex **1** alone in both bacteria and fungi. This shows that gold nanoparticles enhanced the photoinactivation process. The gold nanoparticles used in this study were found to enhance the photoinactivation process in both bacteria and fungi irrespective of their shape. Even though complex **1**–AuNRs gave a slightly larger log reduction compared to complex **1**–AuBPs the statistical analysis showed no significant difference in the results. In the absence of the phthalocyanine the nanoparticles did not show any photothermal effect.

It is expected that the photosensitizers bind to the bacteria or fungal cells to achieve effective photosensitization.[61] The singlet oxygen that is produced by the photosensitizer diffuses into the cells, causing cell death. *C. albicans* cells contain a rather thick layer of chitin and β-glucan which makes the penetration of the photosensitizers into the cell plasma membrane difficult.[13,62] This makes photosensitization of *C. albicans* relatively more difficult compared to *E. coli* and hence lower CFU logs for the former (Table 3).

4. Conclusion

The study shows the potential of an aluminium phthalocyanine and its gold nanoparticle conjugates in photodynamic inactivation of *C. albicans* (fungi) and *E. coli* (bacteria). The conjugates showed an improved photoinactivation by increasing the log reduction of both bacteria and fungi. This is due to increased singlet oxygen quantum yields in the conjugates compared to the Pc alone. The gold nanoparticles alone did not show any photothermal effects. The study did not show any significant difference between the conjugates of the BPs and NRs. Therefore, this study shows that the conjugation of gold nanoparticles to the phthalocyanine can improve the photosensitisation.

Acknowledgements

This work was supported by the Department of Science and Technology (DST)/Nanotechnology (NIC) and National Research Foundation (NRF) of South Africa through DST/NRF South African Research Chairs Initiative for Professor of Medicinal Chemistry and Nanotechnology and Rhodes University.

Notes and references

1 K. McKenzie, M. Maclean, I. V. Timoshkin, E. Endarko, S. J. MacGregor and J. G. Anderson, Photoinactivation of Bacteria Attached to Glass and Acrylic Surfaces by 405 nm Light: Potential Application for Biofilm Decontamination, *Photochem. Photobiol.*, 2013, **89**, 927–935.

2 J. Almeida, J. P. C. Tome, M. G. P. M. S. Neves, A. C. Tome, J. A. S. Caveleiro, A. Cunha, L. Costa, M. A. F. Faustino and A. Almeida, Photodynamic inactivation of multidrug-resistant bacteria in hospital wastewaters: influence of residual antibiotics, *Photochem. Photobiol. Sci.*, 2014, **13**, 626–633.

3 P. Eggimann, J. Garbino and D. Pittet, Epidemiology of Candida species infections in critically ill non-immunosuppressed patients, *Lancet Infect. Dis.*, 2003, **3**, 685–702.

4 L. Ryskova, V. Buchta and R. Slezak, Photodynamic Antimicrobial Therapy, *Cent. Eur. J. Biol.*, 2010, **5**, 400–406.

5 P. Calzavara-Pinton, M. Rossi, R. Sala and M. Venturini, Photodynamic Antifungal Chemotherapy, *Photochem. Photobiol.*, 2012, **88**, 512–522.

6 Y. Nitzan, M. Gutterman, Z. Malik and B. Ehrenberg, inactivation of gram-negative bacteria by photosensitized porphyrins, *Photochem. Photobiol.*, 1992, **55**, 89–96.

7 M. R. Hamblin and T. Hasan, Photodynamic therapy: A new antimicrobial approach to infectious disease?, *Photochem. Photobiol. Sci.*, 2004, **3**, 436–450.

8 M. B. Spesia, M. Rovera and E. N. Durantini, Photodynamic inactivation of Escherichia coli and Streptococcus mitis by cationic zinc(II) phthalocyanines in media with blood derivatives, *Eur. J. Med. Chem.*, 2010, **45**, 2198–2205.

9 A. Segalla, C. D. Borsarelli, S. E. Braslavsky, J. D. Spikes, G. G. Roncucci, D. Dei, G. Chiti, G. Jori and E. Reddi, Photophysical, photochemical and antibacterial photosensitizing properties of a novel octacationic Zn(II)-phthalocyanine, *Photochem. Photobiol. Sci.*, 2002, **1**, 641–648.

10 V. Kussovski, V. Mantareva, I. Angelou, P. Orozova, D. Wöhrle, G. Schnurpfeil, E. Borisova and L. Auramov, Photodynamic inactivation of *Aeromonas hydrophila* by cationic phthalocyanines with different hydrophobicity, *FEMS Microbiol. Lett.*, 2009, **294**, 133–140.

11 A. Minnock, D. I. Vernon, J. Schofield, J. Griffiths, J. H. Parish and S. B. Brown, Photoinactivation of bacteria. Use of a cationic water-soluble zinc phthalocyanine to photoinactivate both gram-positive and gram-negative bacteria, *J. Photochem. Photobiol., B*, 1996, **32**, 159–164.

12 D. A. Caminos, M. B. Spesia, P. Pons and E. N. Durantini, Mechanisms of Escherichia coli photodynamic inactivation by an amphiphilic tricationic porphyrin and 5,10,15,20-tetra(4-N,N,Ntrimethylammoniumphenyl) porphyrin, *J. Photochem. Photobiol.*, 2008, **7**, 1071–1078.

13 M. A. Di Palma, M. G. Alvarez, A. L. Ochoa, M. E. Milanesio and E. N. Durantini, Optimization of cellular uptake of zinc(II) 2,9,16,23-tetrakis[4-(N-methylpyridyloxy)]phthalocyanine for maximal photoinactivation of Candida albicans, *Fungal Biol.*, 2013, **117**, 744–751.

14 T. P. Mthethwa, Y. Arslanoglu, E. Antunes and T. Nyokong, Photophysical behaviour of cationic 2-(dimethylamino) ethanethio tetrasubtituted phthalocyanine complexes in the presence of gold nanoparticles, *Polyhedron*, 2012, **38**, 169–177.

15 M. Managa, M. A. Idowu, E. Antunes and T. Nyokong, Photophysicochemical behavior and antimicrobial activity of dihydroxosilicontris(diaquaplatinum)octacarboxyphthalocyanine, *Spectrochim. Acta, Part A*, 2014, **125**, 147–153.
16 N. Masilela, E. Antunes and T. Nyokong, Axial coordination of zinc and silicon phthalocyanines to silver and gold nanoparticles: an investigation of their photophysicochemical and antimicrobial behavior, *J. Porphyrins Phthalocyanines*, 2013, **17**, 417–430.
17 B. Duncan, C. Kim and V. M. Rotello, The forthcoming applications of gold nanoparticles in drug and gene delivery systems, *J. Controlled Release*, 2011, **149**, 65–71.
18 L. He, M. D. Musick, S. R. Nicewarner, F. G. Salinas, S. J. Benkovic, M. J. Natan and C. D. Keating, Colloidal Au-Enhanced Surface Plasmon Resonance for Ultrasensitive Detection of DNA Hybridization, *J. Am. Chem. Soc.*, 2000, **122**, 9071–9077.
19 N. J. Durr, T. Larson, D. K. Smith, B. A. Korgel, K. Sokolov and A. Ben-Yakar, Two-Photon Luminescence Imaging of Cancer Cells Using Molecularly Targeted Gold Nanorods, *Nano Lett.*, 2007, **7**, 941–945.
20 R. Bhattacharya, C. R. Patra, R. Verma, S. Kumar, P. R. Greipp and P. Mukherjee, Gold Nanoparticles Inhibit the Proliferation of Multiple Myeloma Cells, *Adv. Mater.*, 2007, **19**, 711–716.
21 T. A. EI-Brolossy, T. Abdallah, M. B. Mohamed, S. Abdallah, K. Easawi, S. Negm and H. Talaat, Shape and size dependence of the surface plasmon resonance of gold nanoparticles studied by Photoacoustic technique, *Eur. Phys. J. Special Topics*, 2008, **153**, 361–364.
22 G. Zhang, J. B. Jasinski, J. L. Howell, D. Patel, D. P. Stephens and A. M. Godin, Tunability and stability of gold nanoparticles obtained from chloroauric acid and sodium thiosulfate reaction, *Nanoscale Res. Lett.*, 2012, **7**, 339.
23 D. C. Hone, P. I. Walker, R. Evans-Gowing, S. Fitzgerald, A. Beeby, I. Chamber, M. J. Cook and D. A. Russel, Generation of Cytotoxic Singlet Oxygen via Phthalocyanine-Stabilized Gold Nanoparticles: A Potential Delivery Vehicle for Photodynamic Therapy, *Langmuir*, 2002, **18**, 2985–2987.
24 S. Tombe, E. Antunes and T. Nyokong, The photophysical and photochemical behaviour of coumarin-derivatized zinc phthalocyanine when conjugated with gold nanoparticles and electrospun into polymer fibers, *New J. Chem.*, 2013, **37**, 679–689.
25 X. Huang and M. A. EI-Sayed, Plasmonic photo-thermal therapy (PPTT), *Alexandria J. Med.*, 2011, **47**, 1–9.
26 S. Perni, P. Prokopovich, J. Pratten, I. P. Parkin and M. Wilson, Nanoparticles: their potential use in antibacterial photodynamic therapy, *Photochem. Photobiol. Sci.*, 2011, **10**, 712–720.
27 M. Chen, R. Liu and D. P. Tsai, A Versatile Route to the Controlled Synthesis of Gold Nanostructures, *Cryst. Growth*, 2009, **9**, 2079–2087.
28 N. Kuznetsova, E. A. Makarova, S. N. Dashkevich, N. S. Gretsova, E. A. Kalmykova, V. M. Negrimovsky, O. L. Kaliya and E. A. Lukyanets, Relationship between the photochemical properties and structure of porphyrins and related compounds, *Russ. J. Gen. Chem.*, 2000, **70**, 133–140.
29 I. Scalise and N. E. Durantini, Synthesis, properties, and photodynamic inactivation of Escherichia coli using a cationic and a noncharged Zn(II) pyridyloxyphthalocyanine derivative, *Bioorg. Med. Chem.*, 2005, **13**, 3037–3045.
30 E. A. Dupoy, D. Lazzeri and E. N. Durantini, Photodynamic activity of cationic and non-charged Zn(II) tetrapyridinoporphyrazine derivatives: biological consequences in human erythrocytes and *Escherichia coli*, *Photochem. Photobiol. Sci.*, 2004, **3**, 992–998.
31 V. Mantareva, V. Kussovski, I. Angelov and S. Dimitrov, Advance photodynamic inactivation of dental pathogenic microorganisms with water-soluble and cationic phthalocyanines, in *Science against microbial pathogens: Communicating Current Research and Technological Advances*, ed. A. Mendez-Vilas, Formatex, 2011, vol. 1, pp. 650–661.
32 L. Ryskova, V. Buchta, M. Karaskova, J. Rakusan, J. Cerny and R. Siezak, In vitro antimicrobial activity of light-activated Phthalocyanines, *Cent. Eur. J. Biol.*, 2013, **8**, 168–177.
33 M. Durmuş, S. Yeşilot and V. Ahsen, Separation and mesogenic properties of tetraalkoxy-substituted phthalocyanine isomers, *New J. Chem.*, 2006, **30**, 675–678.
34 A. Kotiaho, R. Lahtinen, A. Efimov, H. K. Metsberg, E. Sariola, H. Lehtivuori, N. V. Tkachenko and H. Lemmetyinen, Photoinduced Charge and Energy Transfer in Phthalocyanine-Functionalized Gold Nanoparticles, *J. Phys. Chem. C*, 2010, **114**, 162–168.
35 M. Liu and P. Guyot-Sionnest, Mechanism of Silver(I)-Assisted Growth of Gold Nanorods and Bipyramids, *J. Phys. Chem. B.*, 2005, **109**, 22192–22200.
36 C. J. Orendorff and C. J. Murphy, Quantitation of metal content in the silver-assisted growth of gold nanorods, *J. Phys. Chem. B.*, 2006, **110**, 3990–3994.
37 D. J. Lewis, T. M. Day, J. V. MacPherson and Z. Pikramenou, Luminescent nanobeads: attachment of surface reactive Eu (III) complexes to gold nanoparticles, *Chem. Commun.*, 2006, 1433–1435.
38 T. Hauck, in A Statistical Model for the Estimation of Gold Nanorod Extinction Coefficients, Term report, University of Toronto, 2005.
39 H. D. Hill, J. E. Millstone, M. J. Banholzer and C. A. Mirkin, The role radius of curvature plays in thiolated oligonucleotide loading on gold nanoparticles, *ACS Nano*, 2009, **3**, 418–424.
40 R. Schmidt, E. McNellis, W. Freyer, D. Brete, T. Grebel, C. Gahl, K. Reuter and M. Weinelt, Azobenzene-functionalized alkanethiols in self-assembled monolayers on gold, *Appl. Phys. A*, 2008, **93**, 267–275.
41 K. Heister, M. Zharnikov, M. Grunze and L. S. O. Johansson, Adsorption of Alkanethiols and Biphenylthiols on Au and Ag Substrates: A High-Resolution X-ray Photoelectron Spectroscopy Study, *J. Phys. Chem. B*, 2001, **105**, 4058–4061.

42 M. Zharnikov, S. Frey, K. Heister and M. Grunze, Modification of Alkanethiolate Monolayers by Low Energy Electron Irradiation: Dependence on the Substrate Material and on the Length and Isotopic Composition of the Alkyl Chains, *Langmuir*, 2000, **16**, 2697–2705.

43 D. G. Castner, K. Hinds and D. W. Grainger, X-ray photoelectron spectroscopy sulfur 2p study of organic thiol and disulfide binding interactions with gold surfaces, *Langmuir*, 1996, **12**, 5083–5086.

44 D. Nilsson, S. Watcharinyanon, M. Eng, L. Li, E. Moons, L. S. O. Johansson, M. Zharnikov, A. Shaporenko, B. Albinson and J. Martensson, Characterization of Self-Assembled Monolayers of Oligo(phenyleneethynylene) Derivatives of Varying Shapes on Gold: Effect of Laterally Extended π-Systems, *Langmuir*, 2007, **23**, 6170–6181.

45 K. Artyushlcova, B. Kiefer, B. Halevl, A. Knop-Gericke, R. Schlogl and P. Atanassov, Density functional theory calculations of XPS binding energy shift for nitrogen-containing graphene-like structures, *Chem. Commun.*, 2013, **49**, 2539–2541.

46 Y. Zhong, M. Jaidann, Y. Zhang, G. Zhang, H. Liu, M. I. Ionescu, R. Li, X. Sun, H. Abou-Rachid and L. Lussier, Synthesis of high nitrogen doping of carbon nanotubes and modeling the stabilization of filled DAATO@CNTs (10,10) for nanoenergetic materials, *J. Phys. Chem. Solids*, 2010, **71**, 134–139.

47 L. Chen, P. Peng, L. Lin, T. C. K. Yang and C. Huang, Facile Preparation of Nitrogen-Doped Activated Carbon for Carbon Dioxide Adsorption, *Aerosol Air Qual. Res.*, 2014, **14**, 916–927.

48 Z. Zhou and Y. Huang, Synthesis of LiFePO4/C cathode materials by carbothermal reduction method using two kinds of Fe3+ precursors, *J. Phys. Conf. Ser.*, 2009, **188**, 012012.

49 Y. Luo, Preparation of silver nanoparticles by heating a quaternary ammonium polyelectrolyte-AgNO3 aqueous solution in basic conditions, *Indian J. Chem.*, 2007, **46A**, 1266–1269.

50 D. Dorjnamjin, M. Ariunaa and Y. K. Shim, Synthesis of Silver Nanoparticles Using Hydroxyl Functionalized Ionic Liquids and Their Antimicrobial Activity, *Int. J. Mol. Sci.*, 2008, **9**, 807–820.

51 W. Huang, S. Chen, Y. Liu, H. Fu and G. Wu, The controlled synthesis of stable gold nanoparticles in quaternary ammonium ionic liquids by simple heating, *Nanotechnology*, 2011, **22**, 025602, (7 pages).

52 W. A. Gole and C. J. Murphy, Seed-Mediated Synthesis of Gold Nanorods: Role of the Size and Nature of the Seed, *Chem. Mater.*, 2004, **16**, 3633–3640.

53 K. Heister, M. Zharnikov, M. Grunze, L. S. O. Johansson and A. Ulman, Characterization of X-ray Induced Damage in Alkanethiolate Monolayers by High-Resolution Photoelectron Spectroscopy, *Langmuir*, 2001, **17**, 8–11.

54 Y. W. Yang and L. J. Fan, High-Resolution XPS Study of Decanethiol on Au(111): Single Sulfur–Gold Bonding Interaction, *Langmuir*, 2002, **18**, 1157–1164.

55 N. R. Tiwari, A. Rathore, A. Prabhune and S. K. Kulkarni, Gold Nanoparticles for Colorimetric detection of hydrolysis of antibiotics by penicillin G acylase, *Adv. Biosci. Biotechnol.*, 2010, **1**, 322–329.

56 S. Vukovic, S. Corni and B. Mennucci, Fluorescence Enhancement of Chromophores Close to Metal Nanoparticles. Optimal Setup Revealed by the Polarizable Continuum Model, *J. Phys. Chem. C*, 2009, **113**, 121–133.

57 A. R. Monahan, J. A. Brado and F. A. DeLuca, Dimerization of a copper(II)-phthalocyanine dye in carbon tetrachloride and benzene, *J. Phys. Chem.*, 1972, **76**, 446–449.

58 S. Perni, C. Piccirillo, A. Kafizas, M. Uppal, J. Pratten, M. Wilson and I. P. Parkin, Antibacterial Activity of Light-Activated Silicone Containing Methylene Blue and Gold Nanoparticles of Different Sizes, *J. Cluster Sci.*, 2010, **21**, 427–438.

59 E. S. Tuchina, V. V. Tuchin, B. N. Khlebtsov and N. G. Khlebtsov, Phototoxic effect of conjugates of plasmon-resonance nanoparticles with indocyanine green dye on *Staphylococcus aureus* induced by IR laser radiation, *Quantum Electron.*, 2011, **41**, 354–359.

60 I. Maliszewska, A. Lesniewska, J. Olesiak-Banska, K. Matczyszyn and M. Samoc, Biogenic gold nanoparticles enhance methylene blue-induced phototoxic effect on Staphylococcus epidermidis, *J. Nanopart. Res.*, 2014, **16**, 1–16.

61 S. George and A. Kishen, Influence of Photosensitizer Solvent on the Mechanisms of Photoactivated Killing of Enterococcus faecalis, *Photochem. Photobiol.*, 2008, **84**, 734–740.

62 M. Osumi, The ultrastructure of yeast: Cell wall structure and formation, *Micron*, 1998, **29**, 207–233.

